Experimental Chaos from Non-Autonomous Electronic Circuits

M. Lakshmanan; K. Murali

Philosophical Transactions: Physical Sciences and Engineering, Vol. 353, No. 1701, Chaotic Behaviour in Electronic Circuits (Oct. 16, 1995), 33-46.

Stable URL:
http://links.jstor.org/sici?sici=0962-8428%2819951016%29353%3A1701%3C33%3AECFNEC%3E2.0.CO%3B2-Q

Philosophical Transactions: Physical Sciences and Engineering is currently published by The Royal Society.

Experimental chaos from non-autonomous electronic circuits

By M. Lakshmanan and K. Murali

Centre for Nonlinear Dynamics, Department of Physics, Bharathidasan University, Tiruchirapalli 620 024, India

Nonlinear non-autonomous electronic circuits are veritable tools to study chaotic dynamics. Considering piecewise-linear non-autonomous circuits containing only one nonlinear element, namely a *nonlinear resistor*, we show that even lower dimensional circuits can exhibit all the fascinating aspects of chaos. In particular, we study the chaotic behaviour of the simplest dissipative second-order circuit of Murali, Lakshmanan and Chua and the extremely simple first-order circuit with a 'jump-rule' proposed by Tang, Mees and Chua.

1. Introduction

The study of nonlinear electronic circuits is a convenient framework to undertake systematic exploration of fundamental mechanisms underlying the onset of chaos. Over the past two decades, piecewise-linear circuits, either of autonomous or non-autonomous nature, have become simple yet powerful models for studying various bifurcation structures and chaos phenomenon in nonlinear dynamics. A variety of nonlinear electronic circuits which exhibits chaos has been reported in the literature in recent times, both in autonomous and non-autonomous cases (Azzouz *et al.* 1983; Chua 1992; Linsay 1981; Madan 1993; Matsumoto *et al.* 1986; Murali & Lakshmanan 1991, 1993; Murali *et al.* 1994*a*, *b*). In the present contribution, we concentrate our attention on only two important, but very simple, non-autonomous electronic circuits and critically examine their chaotic dynamics through experimental results, numerical simulations and analytical discussions.

Higher-order nonlinear non-autonomous circuits are already well studied in the literature (Madan 1993; Murali & Lakshmanan 1991, 1993). For example, the driven Chua's circuit, which is fourth order in nature, has been investigated as a black box exhibiting a rich variety of bifurcation and chaos phenomena, ranging from period doubling route to chaos to quasi-periodicity, intermittency, period adding sequences and so on, as well as a model system for studying control and synchronization (Murali & Lakshmanan 1991, 1993). A simplified third-order version also exhibits similar behaviour both experimentally and numerically (Murali 1994).

In this paper we wish to point out that even a much simpler second-order dissipative nonlinear circuit, consisting Chua's diode as the only nonlinear element, suggested by Murali *et al.* (1994*a*, *b*), can exhibit a rich variety of bifurcation and chaos phenomena. The details are given in § 2. Further, interestingly even a first-order circuit equation, but with a 'jump-rule' and a piecewise-linear (V–I) characteristic curve leading to an one-dimensional shift map, can exhibit chaos, as shown by Tang

Phil. Trans. R. Soc. Lond. A (1995) **353**, 33–46
Printed in Great Britain

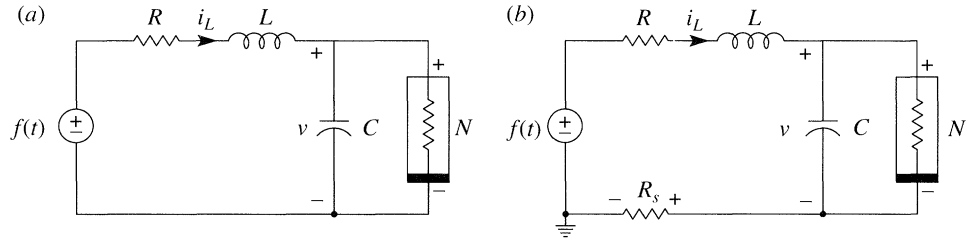

Figure 1. (*a*) Circuit realization of the simple non-autonomous MLC circuit. Here N is the Chua's diode. (*b*) Experimental circuit model with the current sensing resistor R_s. Here $R = 1340\ \Omega$, $L = 18$ mH, $C = 10$ nf, $R_s = 20\ \Omega$ and frequency of the signal source is 8890 Hz.

et al. (1983). The construction and behaviour of this circuit is given in § 3. Finally, a summary of the results is given in § 4.

2. Murali–Lakshmanan–Chua (MLC) circuit

One need not consider higher-order non-autonomous nonlinear circuits to observe chaos but it is sufficient if it is of second-order in nature (Chua *et al.* 1987). In the following we present the details of such a simple and novel second-order non-autonomous chaotic circuit of figure 1 whose only nonlinear element is a Chua's diode. Linsay (1981) had demonstrated chaos experimentally by driving a series circuit made up of a linear resistor, a linear inductor and a varactor diode with a sinusoidal voltage source. However, even though this physical circuit contains only three circuit elements, the circuit model used for computer simulation in (Azzouz *et al.* 1983) contains six circuit elements and the associated nonlinearities are exponential functions, thereby making any mathematical analysis intractable. However, the present circuit of figure 1 proposed by Murali *et al.* (1994*a*, *b*) is much simpler from a circuit theoretic point of view due to the presence of only one nonlinear resistor, namely, the Chua's diode, which is conceptually a much simpler circuit element than a nonlinear capacitor.

(*a*) *Experimental realization*

The circuit realization of the simple non-autonomous MLC circuit is shown in figure 1*a*. It contains a capacitor, an inductor, a linear resistor, an external periodic forcing and only one nonlinear element, namely, the Chua's diode (N) (Cruz *et al.* 1992; Kennedy 1992). To measure the inductor current i_L in our experiments, we insert a small current sensing resistor R_s as shown in figure 1*b*. In the corresponding computer simulations, this resistor is simply added to the resistor R. By applying Kirchhoff's laws to this circuit, the governing equations for the voltage v across the capacitor C and the current i_L through the inductor L are represented by the following set of two first-order non-autonomous differential equations:

$$C\frac{dv}{dt} = i_L - g(v), \quad L\frac{di_L}{dt} = -Ri_L - R_s i_L - v + f\sin(\Omega t), \tag{1}$$

where $g(\cdot)$ is a piecewise-linear function defined by Chua *et al.* (1987)

$$g(v_R) = G_b v_R + 0.5(G_a - G_b)[|v_R + B_p| - |v_R - B_p|], \tag{2}$$

which is the mathematical representation of the characteristic curve of Chua's diode (see figure 2). The slopes of the inner and outer regions are G_a and G_b, while B_p

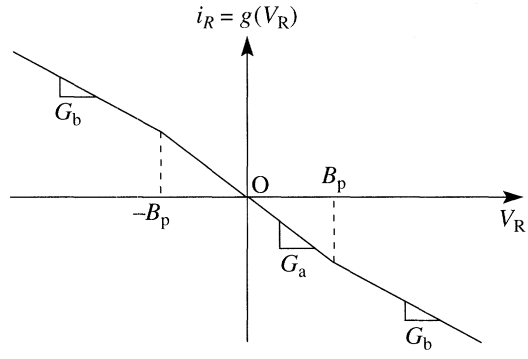

Figure 2. Characteristic curve of the Chua's diode.

indicates break points. In equation (1) f is the amplitude and Ω is the angular frequency of the external periodic force. The parameters of the circuit elements are fixed as $C = 10$ nF, $L = 18$ mH, $R = 1340\ \Omega$, $R_s = 20\ \Omega$ and the frequency ($= \Omega/2\pi$) of the external forcing source is 8890 Hz.

(*b*) *Stability analysis*

The actual values of G_a, G_b and B_p of equation (2) are fixed as -0.76 ms, -0.41 ms and 1.0 V respectively (Kennedy 1992). Rescaling equation (1) as $v = xB_p$, $i_L = GyB_p$, $G = 1/R$, $\omega = \Omega C/G$ and $t = \tau C/G$ and then redefining τ as t the following set of normalized equations are obtained:

$$\dot{x} = y - g(x), \quad \dot{y} = -\beta y - \nu\beta y - \beta x + F\sin(\omega t) \qquad (\dot{} = \mathrm{d}/\mathrm{d}t), \tag{3}$$

where $\beta = (C/LG^2)$, $\nu = GR_s$, and $F = (f\beta/B_p)$. Obviously $g(x) = bx + 0.5(a - b)[|x + 1| - |x - 1|]$, or

$$g(x) = \begin{cases} bx + a - b, & x \geqslant 1, \\ ax, & |x| \leqslant 1, \\ bx - a + b, & x \leqslant -1. \end{cases} \tag{4}$$

Here $a = G_a/G$, $b = G_b/G$. Now the dynamics of equation (3) depends on the parameters ν, β, a, b, ω and F. The experimental circuit parameters used in the previous section are then rescaled as $\beta = 1$, $\nu = 0.015$, $a = -1.02$, $b = -0.55$ and $\omega = 0.75$.

One can easily establish that a unique equilibrium (x_0, y_0) for equation (3) exists in each of the following three subsets,

$$\left.\begin{aligned} D_1 &= \{(x,y)|x > 1\} : \boldsymbol{P}^+ = (-k_1, -k_2), \\ D_0 &= \{(x,y)||x| < 1\}|\boldsymbol{O} = (0,0), \\ D_{-1} &= \{(x,y)|x < -1\}|\boldsymbol{P}^- = (k_1, k_2), \end{aligned}\right\} \tag{5}$$

where $k_1 = \sigma(a - b)/(\beta + \sigma b)$, $k_2 = \beta(b - a)/(\beta + \sigma b)$ and $\sigma = \beta(1 + \nu)$. We also note that the parameters k_1 and k_2 for the present case can be re-expressed as $k_1 = (1 + \nu)(a - b)/(1 + (1 + \nu)b)$ and $k_2 = (b - a)/(1 + (1 + \nu)b)$.

In each of the regions D_1, D_0 and D_{-1}, equation (3) is linear when $F = 0$. It is then easy to see that the stability determining eigenvalues for the equilibrium point

$\boldsymbol{O} \in D_0$ are calculated from the matrix

$$\boldsymbol{A}_0 = \boldsymbol{A}(\beta, \sigma, a) = \begin{bmatrix} -a & 1 \\ -\beta & -\sigma \end{bmatrix} \quad \text{as} \quad \lambda_1 = 0.1904 \quad \text{and} \quad \lambda_2 = -0.1854,$$

a hyperbolic fixed point (*unstable*). Similarly, the matrix

$$\boldsymbol{A}_0 = \boldsymbol{A}(\beta, \sigma, b) = \begin{bmatrix} -b & 1 \\ -\beta & -\sigma \end{bmatrix}$$

associated with the regions D_1 and D_{-1} has a pair of complex-conjugate eigenvalues $(\lambda_1, \lambda_2 = \lambda_1^*)$ with negative real part, like $\lambda_1 = -0.2325+\mathrm{i}(0.623)$ and $\lambda_2 = -0.2325-\mathrm{i}(0.623)$, which indicates that $\boldsymbol{P}^+$ and $\boldsymbol{P}^-$ are stable spiral fixed points (Matsumoto *et al.* 1986). Naturally these fixed points can be observed depending upon the initial condition $x(0)$ and $y(0)$ of equation (3) when $F = 0$. As the forcing signal is included $(F > 0)$ these fixed points give rise to limit cycles through Hopf bifurcation and as F is increased further the system exhibits period doubling bifurcations from the period-1 limit cycle to chaos as discussed below.

(*c*) *Explicit analytical solutions*

Actually equation (3) can be explicitly integrated in terms of elementary functions in each of the three regions D_0, D_1 and D_{-1} and matched across the boundaries to obtain the full solution as shown below.

It is quite easy to see that in each one of the regions D_0, D_{+1}, D_{-1}, equation (3) can be represented as a single second-order inhomogeneous linear differential equation for the variable $y(t)$ as

$$\ddot{y} + (\beta + \beta\nu + \mu)\dot{y} + (\beta + \mu\beta\nu + \beta\mu)y = \Delta + \mu F \sin\omega t + F\omega\cos\omega t, \tag{6}$$

where

$$\mu = a, \quad \Delta = 0 \quad \text{in region } D_0, \tag{7}$$

$$\mu = b, \quad \Delta = \pm\beta(a-b) \quad \text{in region } D_{\pm}. \tag{8}$$

The general solution of equation (6) can be written as

$$y(t) = C^1_{0,\pm}\mathrm{e}^{\alpha_1 t} + C^2_{0,\pm}\mathrm{e}^{\alpha_2 t} + E_1 + E_2\sin\omega t + E_3\cos\omega t, \tag{9}$$

where $C^1_{0,\pm}$ and $C^2_{0,\pm}$ are integration constants in the appropriate regions D_0, $D_{\pm}$ and

$$\left.\begin{aligned} &\alpha_1 = \tfrac{1}{2}(-A + \sqrt{(A^2 - 4B)}), \quad \alpha_2 = \tfrac{1}{2}(-A - \sqrt{(A^2 - 4B)}), \\ &E_1 = 0 \quad \text{in region } D_0 \text{ and } E_1 = \Delta/B \text{ in region } D_{\pm}, \\ &E_2 = (F\omega^2(A-\mu) + \mu F B)/(A^2\omega^2 + (B-\omega^2)^2), \\ &E_3 = F\omega(B - \omega^2 - \mu A)/(A^2\omega^2 + (B-\omega^2)^2), \\ &A = \beta + \beta\nu + \mu, \quad B = \beta + \mu\beta\nu + \beta\mu. \end{aligned}\right\} \tag{10}$$

Knowing $y(t)$, $x(t)$ can be obtained from (3) as

$$\begin{aligned} x(t) &= (1/\beta)\{-\dot{y} - \beta y(1+\nu) + F\sin\omega t\}, \\ &= (1/\beta)\{-\dot{y} - \sigma y + F\sin\omega t\}, \\ &= (1/\beta)\{-C^1_{0,\pm}\mathrm{e}^{\alpha_1 t}(\alpha_1 + \sigma) - C^2_{0,\pm}\mathrm{e}^{\alpha_2 t}(\alpha_2 + \sigma) \\ &\qquad -(\cos\omega t)(E_2\omega + E_3\sigma) + (\sin\omega t)(F - E_2\sigma + E_3\omega) - E_1\sigma\}. \end{aligned} \tag{11}$$

Table 1. *Summary of bifurcation phenomena of equation (3)*

amplitude (F)	description of attractor	figure 3*b*
$0 < F \leqslant 0.071$	period-1 limit cycle	(i)
$0.071 < F \leqslant 0.089$	period-2 limit cycle	(ii)
$0.089 < F \leqslant 0.093$	period-4 limit cycle	(iii)
$0.093 < F \leqslant 0.19$	chaos	(iv,v)
$0.19 < F \leqslant 0.3425$	period-3 window	(vi)
$0.3425 < F \leqslant 0.499$	chaos	(not included here)
$0.499 < F \leqslant 0.625$	period-3 window	(not included here)
$0.625 < F$	period-1 boundary	(vii)

Thus if we start with the initial condition in D_0 the arbitrary constants C_0^1 and C_0^2 in (9) get fixed. Then $x(t)$ evolves as given in (11) up to either $t = T_1$, when $x(T_1) = 1$ and $\dot{x}(T_1) > 0$ or $t = T_1'$, when $x(T_1') = -1$ and $\dot{x}(T_1') < 0$. Knowing whether $T_1 > T_1'$ or $T_1 < T_1'$ we can determine the next region of interest ($D_\pm$) and the arbitrary constants of the solutions of that region can be fixed by matching the solutions. This procedure can be continued for each successive crossing. In this way explicit solutions can be obtained in each of the regions D_0, $D_\pm$. However, it is clear that sensitive dependence on initial conditions is introduced in each of these crossings at appropriate parameter regimes during the inversion procedure of finding T_1, T_1', T_2, T_2',..., etc., from the solutions. The time instances T_i or T_i's can only be computed numerically.

(*d*) *Experimental and numerical studies*

In order to study the dynamics of this circuit the amplitude f of the forcing signal is used as the bifurcation parameter. By increasing the amplitude from zero upwards, the circuit of figure 1 is found to exhibit experimentally a sequence of bifurcations. Starting from a direct-current equilibrium, the solution bifurcates through a Hopf bifurcation to limit cycle, and then by period-doubling sequences to Chua's one-band attractor, double-band attractor, periodic windows, boundary crisis, etc., as illustrated in figure 3*a* as the forcing strength f varies. Also by using the standard 4th-order Runge–Kutta integration routine we have carried out numerical analysis of (3) with the rescaled circuit parameters of figure 1 as $\beta = 1.0$, $\nu = 0.015$, $a = -1.02$, $b = -0.55$ and $\omega = 0.75$ (Murali *et al.* 1994*a*, *b*), with F as the control parameter. The results are summarized in table 1 and some of them are also exhibited in figure 3*b*.

(*e*) *Chua's diode with single break-point and spiral Chua's attractor*

Figure 3*b*(iv) shows the appearance of spiral Chua's attractor for $F = 0.1$. The invariance of equation (3) under the reflection $(x, y) \rightarrow (-x, -y)$ implies that there is another spiral-type chaotic attractor located symmetrically with respect to the origin, depending upon the initial conditions. The symmetry, in turn, stems from the symmetry of the function $g(\cdot)$ in equation (4). This observation suggests that one attractor should still be present even if one replaces the 3-segment function $g(\cdot)$ of the Chua's diode with the 2-segment function in figure 4. This conjecture is confirmed in figure 5, where the spiral type chaotic attractor is observed with a

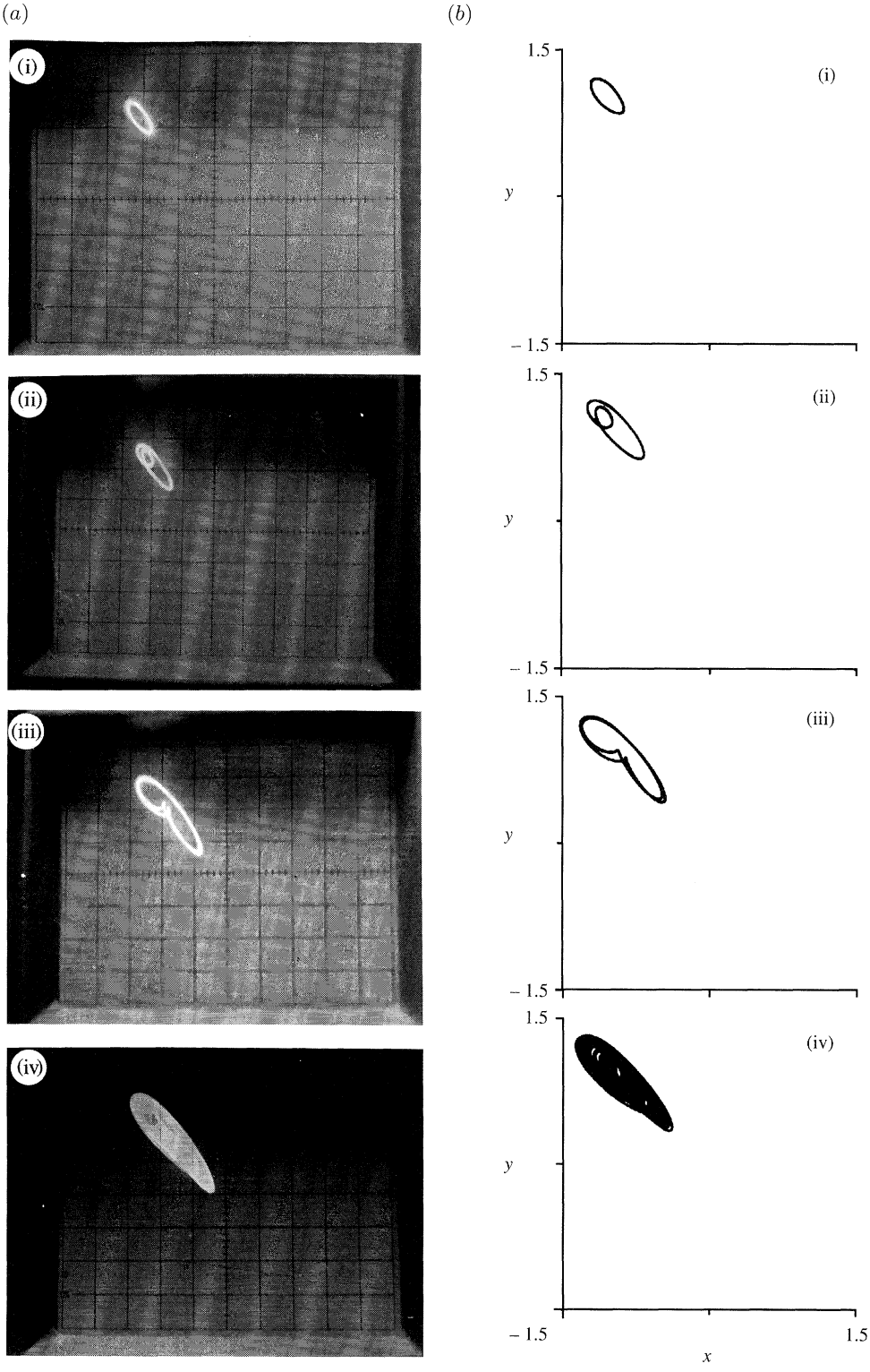

Figure 3. For description see opposite.

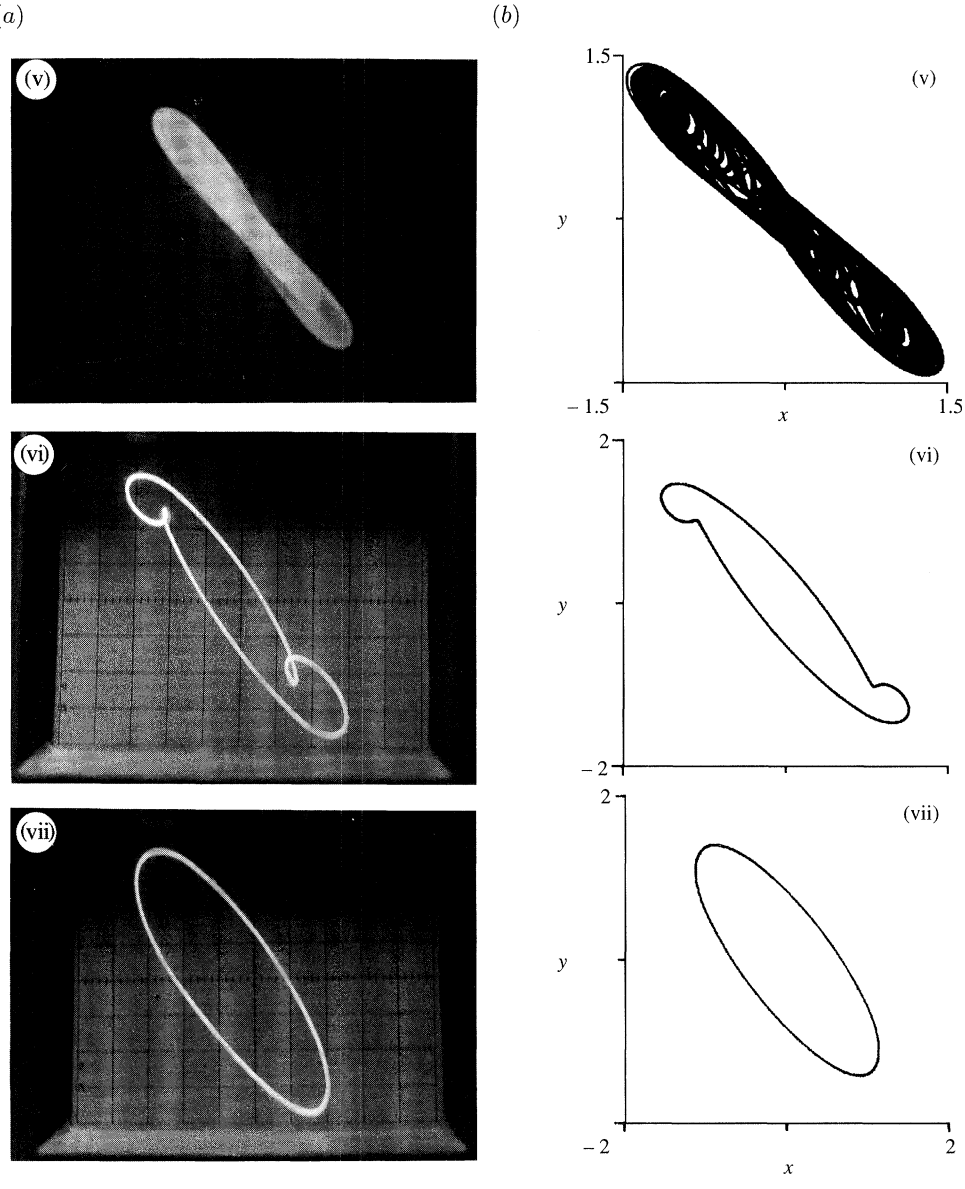

Figure 3. Experimental results and corresponding results of numerical simulations. (*a*) Projection of the trajectories on to the v–v_s ($= R_s i_L$) plane. (*b*) Projection of trajectories on to the x–y plane of equation (3) through numerical simulations. Here f_c is the calculated value of the forcing amplitude using the relation $f_c = FB_p/\beta$. (i) Period-1 limit cycle: (*a*) $f = 0.0365V_{rms}$, (*b*) $F = 0.065$ ($f_c = 0.046V_{rms}$); (ii) Period-2 limit cycle: (*a*) $f = 0.0549V_{rms}$, (*b*) $F = 0.08$ ($f_c = 0.0565V_{rms}$); (iii) Period-4 limit cycle: (*a*) $f = 0.064V_{rms}$, (*b*) $F = 0.091$ ($f_c = 0.06435V_{rms}$); (iv) One-band chaos: (*a*) $f = 0.0723V_{rms}$, (*b*) $F = 0.1$ ($f_c = 0.0707V_{rms}$); (v) Double-band chaos: (*a*) $f = 0.107V_{rms}$, (*b*) $F = 0.15$ ($f_c = 0.106V_{rms}$); (vi) Period-3 window: (*a*) $f = 0.145V_{rms}$, (*b*) $F = 0.2$ ($f_c = 0.1414V_{rms}$); (vii) Period-1 boundary: (*a*) $f = 0.488V_{rms}$; (*b*) $F = 0.7$ ($f_c = 0.495V_{rms}$).

piecewise-linear resistor having only one break-point (see also Sparrow 1981). The mathematical representation of the characteristic curve of the figure 4 can be given

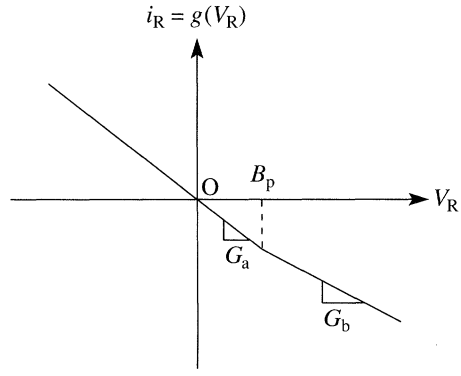

Figure 4. Modified resistor characteristic with a single break point of the Chua's diode.

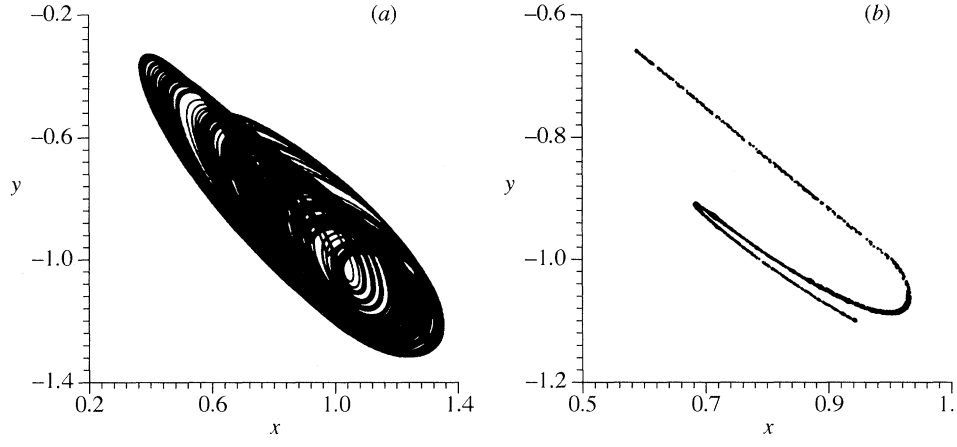

Figure 5. (*a*) Spiral Chua's attractor obtained from equation (3) and equation (12) for $F = 0.1$ with characteristic curve of figure 4. (*b*) Poincaré map of (*a*).

(Chua *et al.* 1987) as

$$g(x) = 0.5(b-a)[|x - B_p| - |B_p| + 0.5(a+b)x, \tag{12}$$

or

$$g(x) = \begin{cases} bx + a - b, & x \geqslant B_p, \\ ax, & x \leqslant B_p. \end{cases} \tag{13}$$

Here $B_p = 1.0$, $a = -1.02$ and $b = -0.55$. However, the experimental realization of the nonlinear resistor with 2-segment characteristic curve is difficult but this can be attained by adding a bias battery in series with the sinusoidal source (Matsumoto *et al.* 1986). Also one can obtain explicit solutions of various regions of operation of equation (3) along with equation (13) as in the 3-segment case.

3. Loss of synchronization and chaos: Tang–Mees–Chua model

In some sense an even more simpler circuit than the MLC circuit, but with a non-monotonic V–I characteristic requiring a 'jump-rule' associated with a first-order differential equation, is the piecewise-linear circuit suggested by Tang, Mees

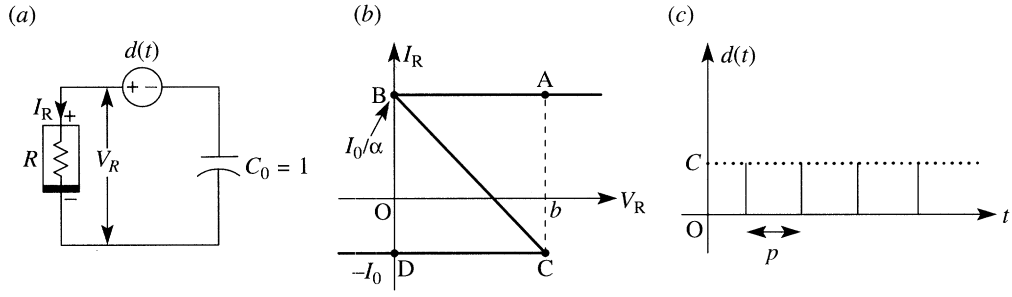

Figure 6. (*a*) The circuit model of the triggered astable oscillator. (*b*) The idealized I_R–V_R characteristic of the nonlinear resistor. (*c*) Narrow periodic trigger pulses.

and Chua (TMC model) (Tang *et al.* 1983). The jump rule of the circuit provides the extra dynamics to make the system chaotic and maps it exactly onto a one-dimensional shift map. The TMC system is essentially an astable multivibrator as in figure 6*a*, whose nonlinear resistor has an idealized piecewise-linear V–I characteristic (figure 6*b*). The circuit of figure 6*a* is triggered by small synchronization trigger pulses of figure 6*c*. Then by very straightforward arguments one can easily see that the loss of synchronization between the unforced oscillator and the forcing signal ultimately leads to chaos.

The operation of the circuit of figure 6*a* proceeds as follows. The nonlinear resistor of figure 6*a* charges capacitor C_0 with current I_0 during the time b/I_0 until it reaches point $C(V_R = b)$. An instantaneous transition from C to A is assumed to occur at this point and thereafter resistor R begins to discharge C_0 with a current equal to $-I_0/\alpha$ during the interval $b\alpha/I_0$. When it reaches $B(V_R = 0)$, during this time another instantaneous transition from B to D is assumed to occur and R starts charging C_0 again.

The assumption that an instantaneous jump from C to A (and from B to D) occurs is called the *jump postulate* or *phenomenon* in circuit theory (Chua *et al.* 1987), and often represents a very realistic model of experimentally observed phenomena. Each boundary point where the jump takes place is called an *impasse point* (Chua *et al.* 1987), and comprehensive theory has been developed to show how an impasse point occurs naturally as a result of idealizations resulting from setting some small but essential circuit parameters (called *parasitics*) to zero (Chua *et al.* 1987). The presence of the triggering signal $d(t)$ may trigger the jump from C to A before the capacitor voltage has reached the threshold b. This occurs if a pulse arrives when the capacitor voltage is rising between the values $b - c$ and b. Otherwise, the triggering pulses have no effect.

If the period p of the signal is slightly smaller than the period q of the free-running multivibrator, all pulses $d(t)$ will trigger the jump and thus the forced multivibrator output is synchronized with $d(t)$. This normal functioning of the oscillator is shown in figure 7. The behaviour of this circuit model can be described by the equation,

$$\dot{x}(t^+) = \begin{cases} I_0, & \text{if } \dot{x}(t) > 0 \text{ and } x(t) + d(t) < b, \\ & \text{or if } x(t) + d(t) \leqslant 0, \\ -I_0/\alpha, & \text{if } \dot{x}(t) < 0 \text{ and } x(t) + d(t) > 0, \\ & \text{or if } x(t) + d(t) \geqslant b, \end{cases} \tag{14}$$

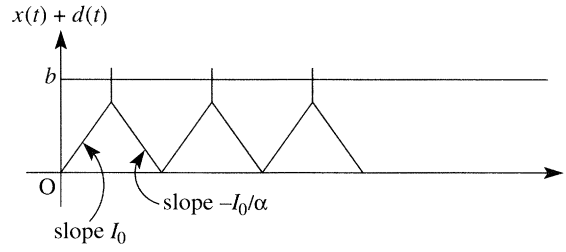

Figure 7. A possible output waveform of figure 6*a*. Slope changes when $x + d$ reaches b from below or 0 from above. Period of $x + d$ is locked on to the period of d. Here x corresponds to the capacitor voltage.

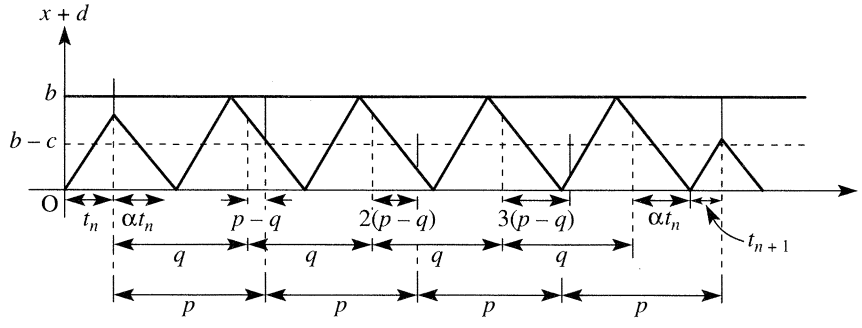

Figure 8. A possible triggered waveform.

where x corresponds to the capacitor voltage and t^+ denotes $\lim_{\epsilon\to 0}(t+\epsilon)$. Now let us assume that the driving signal's period p is slightly longer than the free running period q. Suppose also that $p - q$ is less than c/I_0, the time for x, the capacitor voltage, to rise from its lowest triggerable value to its maximum. Let t_n be the rise time of the nth successfully triggered wave segment. That is when a trigger pulse causes the nth slope change, t_n is the time from the trigger pulse back to when the signal was last zero. With these assumptions, a possible waveform of $x + d$ is plotted in figure 8. If $p-q$ is small, the circuit will not usually be triggered again on the cycle immediately after a successful triggering instead, it will free-run with the triggering pulse shifting a distance $p - q$ on each cycle. From figure 8, it is easy to see that the next successful triggering occurs when

$$(p-q)k \geqslant \alpha t_n + (b-c)/I_0, \tag{15}$$

where k is the smallest integer that satisfies (15) and $(b - c)/I_0$ is the time needed for the capacitor C to be charged from zero to the triggering threshold voltage $b - c$.

Using the notation of figure 8, we get

$$t_{n+1} = (p-q)k - \alpha t_n, \tag{16}$$

and this recurrence relation describes the system fully. Also from the figure, we can easily check that

$$\alpha t_n + (b-c)/I_0 = (k-1)(p-q) + (\alpha t_n + (b-c)/I_0) \bmod (p-q). \tag{17}$$

Eliminating k between (16) and (17) and setting, $\tau_n = t_n - (b - c)/I_0$, we obtain

$$\tau_{n+1} = (p-q) - (\alpha\tau_n + \beta) \bmod (p-q), \tag{18}$$

where β is a constant which we may take to lie in $[0, p-q]$ without loss of generality,

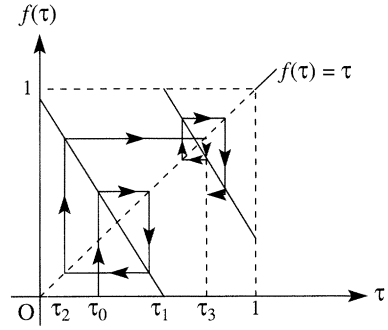

Figure 9. The effect of $f(\tau_n)$. τ_0 is mapped to $f(\tau_0)$. The line $f(\tau) = \tau$ reflects $f(\tau_0)$ into τ-axis. This reflected point becomes τ_1 and the process continues. The mapping and reflecting proceed along the arrows.

because of the modulo$(p - q)$ operation. Also, if $(p - q) = 1$, we finally deduce the equivalent one-dimensional shift map

$$\tau_{n+1} = f(\tau_n) = 1 - (\alpha\tau_n + \beta) \bmod 1. \tag{19}$$

To each time evolution of the circuit there corresponds the sequence τ_n, which is obtained by iterating the function $f(\tau_n)$ on the initial value τ_0. One can analyse these iterations rigorously for different cases $\alpha < 1$, $\alpha = 1$ and $\alpha > 1$ of (19) and the brief description of the results of these cases are as follows. When $\alpha < 1$, the system (19) exhibits fixed point solution (corresponding to period-1 oscillation of the original system). When $\alpha = 1$, period-2 oscillations occur and when $\alpha > 1$ the map (19) exhibits chaotic behaviour. For the case of $\alpha > 1$, all the fixed points of $f(\tau_n)$ are now unstable; moreover iterates f^m of f consists of straight line segments with slope $(-\alpha)^m$ and so fixed points of all periods are unstable. So there can be no stable periodic solutions (see figure 9). Also, the mapping is always locally expansive: nearby points get pulled further and further apart, until eventually they find themselves on opposite sides of a discontinuity of f, corresponding to being in different switching cycles of the original system.

The exponential divergence and sensitive dependence on initial conditions can be rigorously established for this map, by considering an α-nary expansion for the variable x_0 and by defining $x_n = [t_n/(p - q)] \bmod 1$: that is

$$x_0 = \sum_{j=1}^{\infty} x_{0j}\alpha^{-j}, \qquad \text{where } 0 \leqslant x_{0j} < \alpha.$$

It follows from (16) and the fact α is an integer, that $x_{n+1} = (-\alpha x_n) \bmod 1$, which implies

$$x_1 = 1 - \sum_{k=1}^{\infty} x_{0,(k+1)}\alpha^{-k}, \quad x_2 = \sum_{k=1}^{\infty} x_{0,(k+2)}\alpha^{-k}, \ldots$$

$$x_{2n} = \sum_{k=1}^{\infty} x_{0,(k+2n)}\alpha^{-k}, \quad x_{2n+1} = 1 - \sum_{k=1}^{\infty} x_{0,(k+2n+1)}\alpha^{-k}.$$

Thus there is a one-to-one correspondence between the α-nary expansion of x_0 and the sequence $\{x_n\}$. The above equations exhibit that at each iterate, the expansion loses its first digit and is complemented modulo α. Thus for example in the case

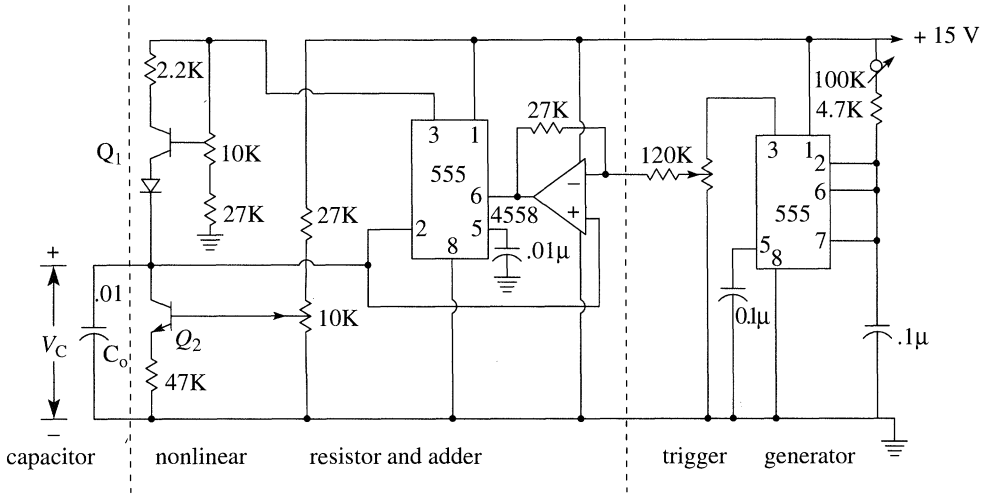

Figure 10. The experimental circuit of the triggered astable oscillator (Tang *et al.* 1983).

$\alpha = 2$ (which is similar to the Bernoulli shift map (McCauley 1993)), the map can be represented as

$$\begin{aligned} 0.0101\ldots &\longrightarrow 0.1010\ldots \qquad \text{(drop first digit)},\\ &\longrightarrow 0.0101\ldots \qquad \text{(subtract from 1)}. \end{aligned}$$

To examine the history of any point, one writes down its α-nary expansion and complement the odd numbered digits modulo α. The digits then give, in order, the kneading intervals visited. Since two nearby initial points will have α-nary strings that differ in an arbitrary manner, beyond a finite number of slots, all informations about the 'nearness' of the points will be lost after a finite number of applications of the map, resulting in random numbers. Thus one sees in a transparent way the onset of chaos.

Finally, to illustrate and confirm the chaotic behaviour predicted above a simple experimental circuit which simulates, almost exactly, the idealized I_R–V_R characteristic in figure 6*b* has been built and studied in Tang *et al.* (1983). The experimental circuit of TMC model is shown in figure 10. A standard integrated circuit module NE555 performs the switching between charging and discharging. The two transistors act as current sources. When the output of NE555 is high, Q_1 overcomes Q_2 and charges C_0. Otherwise Q_1 is OFF and C_0 is discharged by Q_2. The other NE555 generates the triggering signal which is added to the oscillator via an operational amplifier. A typical power spectrum plot depicting the broad spectrum of the resulting triangular waveform v_c from the circuit is shown in figure 11, and thereby confirming the chaotic behaviour of the circuit of figure 6*a*.

Finally, it is worth mentioning that Li & Yorke (1978) have discussed rigorous evidence for chaos (ergodic and expanding) from one-dimensional maps which include the TMC map of equation (19). Also recently, Saito & Oikawa (1993) have proposed a simple piecewise-linear non-autonomous chaotic circuit and proved its chaos generation in the sense of discussions by Li & Yorke (1978).

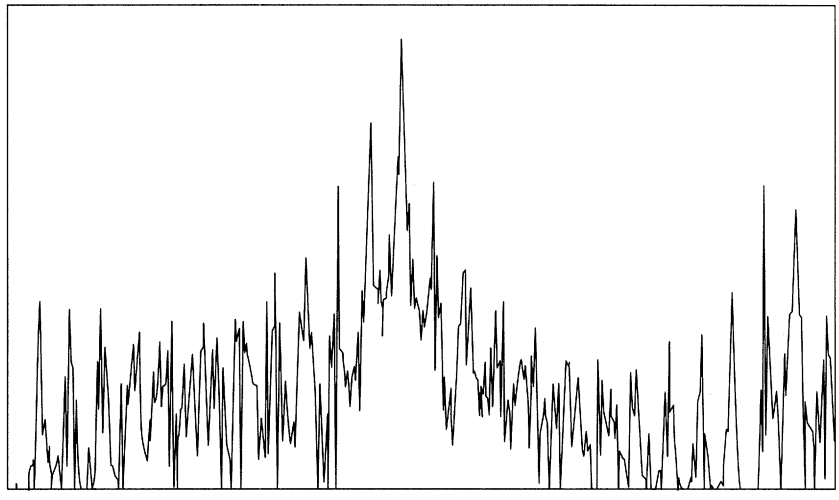

Figure 11. The power spectrum of a typical waveform of v_c (Tang *et al.* 1983).

4. Conclusion

We have given convincing evidence that simple low-dimensional piecewise-linear non-autonomous circuits with *nonlinear resistors* can be ideal models to study chaotic dynamics. As typical examples we examined the chaotic dynamics of the second-order dissipative MLC circuit and the first-order TMC circuit model with a 'jump-rule'. The results show clearly how such simple nonlinear circuits can bring out all the fascinating aspects associated with chaos.

This work has been supported by the Department of Science and Technology, Government of India in the form of a research project.

References

Azzouz, A., Duhr, R. & Hasler, M. 1983 Transition to chaos in a simple nonlinear circuit driven by a sinusoidal voltage source. *IEEE Trans. Circuits Systems* **30**, 913–914.

Chua, L. O., Desoer, C. A. & Kuh, E. S. 1987 *Linear and nonlinear circuits.* Singapore: World Scientific.

Chua, L. O. 1992 The genesis of Chua's circuit. *Arch. Elektronik Übertrag.* **46**, 250–257.

Cruz, J. M. & Chua, L. O. 1992 An IC diode for Chua's circuit. *Int. J. Circuit Theory Applic.* **21**, 309–316.

Kennedy, M. P. 1992 Robust op-amp realization of Chua's circuit. *Frequenz* **46**, 66–80.

Li, T. Y. & Yorke, J. A. 1978 Ergodic transformations from an interval into itself. *Trans. Am. math. Soc.* **235**, 183.

Linsay, P. S. 1981 Period doubling and chaotic behaviour in a driven anharmonic oscillator. *Phys. Rev. Lett.* **47**, 1349–1352.

Madan, R. N. 1993 *Chua's circuit: a paradigm for chaos.* Singapore: World Scientific.

Matsumoto, T., Chua, L. O. & Komuro, M. 1986 The double scroll bifurcations. *Int J. Circuit Theory Applic.* **14**, 117–146.

McCauley, J. L. 1993 *Chaos, dynamics and fractals: an algorithmic approach to deterministic chaos.* Cambridge University Press.

Murali, K. & Lakshmanan, M. 1991 Bifurcation and chaos of the sinusoidally driven Chua's circuit. *Int. J. Bifurc. Chaos* **1**, 369–384.

Murali, K. & Lakshmanan, M. 1993 Chaotic dynamics of the driven Chua's circuit. *IEEE Trans. Circuits Systems* I **40**, 836–840.

Murali, K., Lakshmanan, M. & Chua, L. O. 1994*a* The simplest dissipative non-autonomous chaotic circuit. *IEEE Trans. Circuits Systems* I **41**, 462–463.

Murali, K., Lakshmanan, M. & Chua, L. O. 1994*b* Bifurcation and chaos in the simplest dissipative non-autonomous circuit. *Int. J. Bifurc. Chaos* **4**, 1511–1524.

Murali, K. 1994 Bifurcation, controlling and synchronization of certain chaotic nonlinear electronic circuits. Ph.D. thesis, Bharathidasan University, Tiruchirapalli.

Saito, T. & Oikawa, M. 1993 Chaos and fractals from a forced artificial neural cell. *IEEE Trans. Neural Networks* **4**, 43.

Sparrow, C. T. 1981 Chaos in a 3-dimensional single loop feedback system with a piecewise-linear feedback function. *J. math. Analysis Applic.* **83**, 275–291.

Tang, Y. S., Mees, A. I. & Chua, L. O. 1983 Synchronization and chaos. *IEEE Trans. Circuits Systems* **30**, 620–626.